

# Approach to Autonomous Control in a Multi Domain Environment

Christopher P. Payne, Connor J.D. Keir, Daniel Ballin, Daniel Croul, Ethan K. Waters, Jack Nguyen, Jakson Gardnir, Joshua Smallwood, Rio Thomas, Ross L. Siddins, Timothy Yanner, Topher Rawlings

**Abstract – Autonomous Marine Systems (AMS) are made up of one or multiple autonomous vessels that must coordinate and make decisions based on information detecting in the marine environment. This paper intends to demonstrate the approach pursued by the JCU Robotics team based at James Cook University of Townsville, Australia in designing and controlling an AMS for the RoboNation RobotX International Competition.**

## I. INTRODUCTION

The Parker-McKeough AMS is comprised of two composite systems: the McKeough Uncrewed Surface Vehicle (USV) and the Parker Uncrewed Aerial Vehicle (UAV). The McKeough USV is the designation of JCU Robotics' WAM-V platform, sporting an aerial deployment pad which hosts the Parker UAV quadcopter.

A variety of new tasks were added to ROBOTX 2022 introducing the requirement of UAV capability. These tasks include Task 4 - Wildlife Encounter, Task 8 - UAV Replenishment, and Task 9 - UAV Search and Report. To complete these, the UAV must be autonomously deployed to conduct close area search and report operations with a suite of sensors before retrieval.

## II. DESIGN STRATEGY

### A. McKeough USV

#### 1. General Design Overview

Manoeuvring behaviour of USVs is governed by a common three-level control architecture, composed of path and motion planning, dynamic control, localisation and mapping. Data acquired from perception sensors such as LiDAR, RADAR and cameras advise system behaviour in an intelligent manner from identification of obstacles, features, and mapping of the surrounding environment. The development and investment towards automation of terrestrial, marine and air vehicles has gained considerable interest in recent years for the purpose of minimising risk to human operators. In particular, marine operations ranging from search-and-rescue to oceanographic surveying can be highly volatile due to rapidly changing environmental conditions, which has increased the need for advanced autonomy of USVs.

#### 2. Obstacle Avoidance

To detect buoys and determine their colour, computer vision will be utilised. In the outdoor environment, the unpredictable changes in lighting conditions, reflections from the water, shadows, and background noise will negatively affect the accuracy of the outcome. Therefore, the following steps should be considered to counteract these challenges:

1. Capture image.
2. Apply Gaussian filter to minimise undesired background noise.
3. Transform filtered image into HSV and Lab colour space to detect green and red buoys respectively. Subsequently, apply thresholding (upper and lower bounds) within each channel of its colour space to remove other objects of different colours.
4. Apply open and close morphology to remove salt and pepper noise.
5. Use OpenCV to detect the contour of the threshold image and find the bounding box of the detected obstacles if their contour area is greater than the threshold area.

The threshold parameters can be determined from a HSV and Lab colour thresholder which can be implemented in Python. Specifically, HSV and Lab parameters such as upper and lower bound values are identified based on their colour properties. Subsequently, these threshold values can be imported to the main program for real time operations.

It is assumed that the WAM-V should be able to change direction fast enough in any situation when obstacles are detected. For efficiency purposes of the Python code, it should be sufficient to consider the closest obstacles position of each colour i.e., red and green. If there are multiple obstacles of the same colour detected, only the closest detected red and/or green buoy positions are processed for path planning for efficiency.

The calculation of distance and angle between the camera and detected obstacles in the robotic field is critical for an ASV to navigate its surroundings, thus what follows is a summary of approaches for measuring

distance and angle of detected objects to the camera using a single camera. Distance estimation requires three main parameters, detected pixel height, reference height and distance to the obstacle. Specifically, the mentioned parameters are used to calculate the focal length of the camera and subsequently the estimated distance. Figure 1 depicts the reference height of the captured object (height b), real-time captured image (height a) and actual object height (height h). Using the geometrical relationship between the height (b), height (h) and known distance, the focal length can be calculated using (1). Since the height of the object remains unchanged in object plane, the distance (d) of the object from the camera can be calculated using (2).

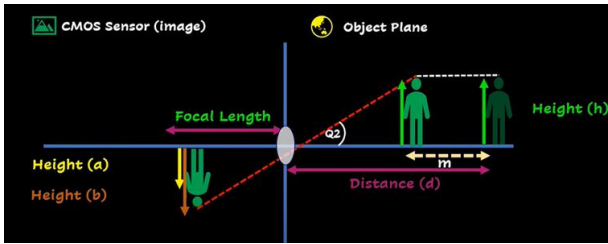


Figure 1 Height of Captured Image vs. Actual Image

$$Focal\ length = \frac{reference\ pixel\ height * known\ distance}{known\ height} \quad (1)$$

$$Estimated\ distance = \frac{known\ height * focal\ length}{real\ time\ pixel\ height} \quad (2)$$

The angle between objects from the camera requires information from the camera's horizontal field of view (HFOV), resolution of the captured object plane and centroid of the detected obstacles. The angle can be calculated using (3). Where  $x$  is the  $x$ -centroid of the obstacle and  $W$  is the width of the captured object plane.

$$Angle = \frac{\left(x - \frac{W}{2}\right) * \frac{HFOV}{2}}{\frac{W}{2}} \quad (3)$$

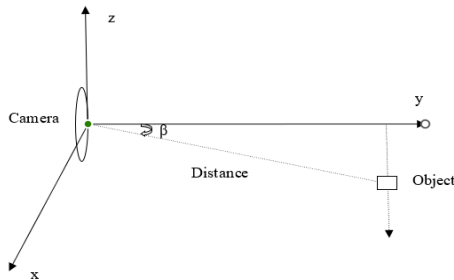


Figure 2 Layout of the Object Plane

### B. Parker UAV

The approach to the design of the UAV was to find the most efficient manner to achieve a craft capable of providing a stabilised platform with a flight duration of approximately 20 minutes and AUW of less than 7kg. After various design simulations and calculations the team arrived on a modified Jormungandr - Midgard Serpent X - Class racing frame - True X quadcopter, with a drive system consisting of four Xnova M4808-700kV, throttle limited to 490kV, fitted with 15x7x3 propellers. This combination allows for a total AUW lift capacity of 5.5kg, for approximately 20 minutes when powered by a 4S6P, 18650, 18000mAh Li-ION battery.

## III. VEHICLE DESIGN

### A. McKeough USV

#### 1. System Identification and Control

Model-based control methods such as sliding mode, model predictive, and model reference adaptive controls have demonstrated superior performance in terms of stability and accuracy, and effort is typically made in improving system identification procedures to estimate hydrodynamic derivatives more accurately.

Identification theory is integral to parameterisation of mathematical models used to represent dynamical systems. For marine vessels hydrodynamic forces and moments are complex functions of the vessel's motion through the fluid and require significant effort to be determined (Grey-box modelling is used).

Grey-box modelling is based on formulating a simple model which captures the most relevant dynamics and characterising unmodelled behaviour as an uncertainty term. The uncertainty terms (hydrodynamic derivatives) are obtained from empirical data using offline or online methods. Manoeuvring theory is used to develop the WAM-V model, with the general manoeuvring equation of motion represented in (4).

$$(M_{RB} + M_A)\dot{v} + (C_{RB}(v) + C_A(v))v + (D_l(v) + D_n(v))v = \tau + \tau_{ext} \quad (4)$$

Where  $M_{RB}$  and  $M_A$  are the rigid-body and added-mass system inertia matrices,  $C_{RB}$  and  $C_A$  are the rigid-body and added mass coriolis and centripetal matrices,  $D_l$  and  $D_n$  are linear and non-linear damping terms,  $\tau$  is a vector of propulsion forces and moments, and  $\tau_{ext}$  is a vector of external disturbances such as wind or current.

The system is over-actuated with four thrusters in 3 degrees of freedom, described by Figure 3. Each propulsion unit is characterised by a thrust force  $T_p$ ,  $T_s$ ,  $T_l$  and  $T_r$  which produce longitudinal and lateral force

components. Yawing moment  $B$  denotes centreline-to-centreline side hull separation while  $L_{cg}$  denotes distance between bow plane of engine pods with respect to centre of gravity.

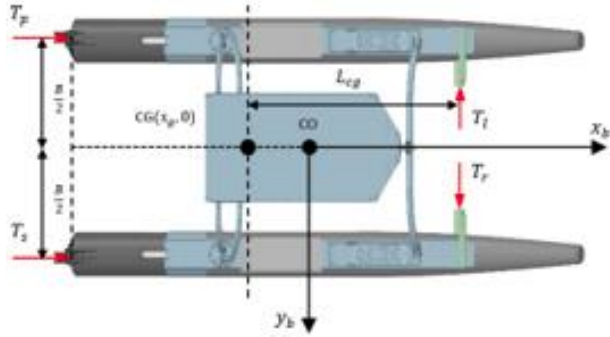


Figure 3 Propulsion system of the WAM-V with thrust produced on port and starboard sides from two fixed aft thrusters, in addition to fore mounted motors on the left and right.

The linear thrust model (5) is used to describe output thrust as a function of input motor command. As demonstrated,  $n$  is input motor command in revolutions per minute (RPM),  $n_{max}$  is maximum rated motor RPM, and  $T_{max}$  is the maximum force produced by motors at full throttle.

$$T = \frac{n}{n_{max}} T_{max} \quad (5)$$

## 2. Communication

Communication between different subsystems is a key element that allows the WAM-V to traverse through its environment safely, efficiently and effectively. Subsystems such as computer vision, path planning subsystem must clearly communicate with the control system of the WAM-V in addition to performing its intended function. These subsystems are processed using Raspberry Pi (RPI), hence, there are various popular methods to communicate between the two such as serial GPIO (general purpose input/output), USB serial and USB-TTL to Rx/Rx. Serial GPIO communication is chosen since the connections only require three low-cost jumpers. A VNC Viewer on PC is required to connect to the Raspberry Pi. There are several viewers available, however Real VNC was used as it is the simplest to set up.

Local Wi-Fi network allows all RPI's on WAM-V to be connected to the same network for remote access and monitoring. Local network will employ Netgear N300 Wireless ADSL2+ Modem Router DGN2200 to provide local network connection between RPI's and PC.

## B. Parker UAV

JCU Robotics' approach to this challenge incorporates a modified Jormungandr Midgard Serpent X-Class racing frame with sensors including the Here3 RTK-enabled GNSS module, an IRLOCK PixyCam precision landing system and a PixyCam RGB Camera.

### 1. Command and Control

The command and control of the UAV is managed by an mRo R15 Pixracer Flight Controller with PX4 protocol via RFD900 modem. The RFD900 is configured as a slave within a Multimodal network between the WAM-V and Ground station and a remote-controlled manual operation fall back.

### 2. Safety Features

Within the design of the UAV, safety was always at the forefront of the approach. For overwater operation considerations, a floatation system capable of handling 7kg was fitted to the frame. A core challenge here was to design the floatation ring high enough to prevent electronics from being submerged while minimising sensor obstruction. Regarding control, precautions such as geofencing capability and a 'Return to Home' function have been implemented for all flight modes.

To reduce the possibility of battery fire, a lithium-ion battery cell was selected rather than the traditional lithium-polymer batteries used in common recreational and commercial UAVs.

## IV. EXPERIMENTAL RESULTS

### A. McKeough USV

#### 1. Indoor Object Detection Experiment Results

The experiment was firstly examined in an indoor environment which would have minimal effects from sunlight and no water reflection presence. It was first to perform colour thresholding to remove all other objects except green and red cones using HSV and Lab programmed colour thresholder, respectively. The resulting threshold HSV and Lab output images are shown in Figures 4 and 5. The threshold values are shown in Table 1. These values are subject to change with different environmental conditions.

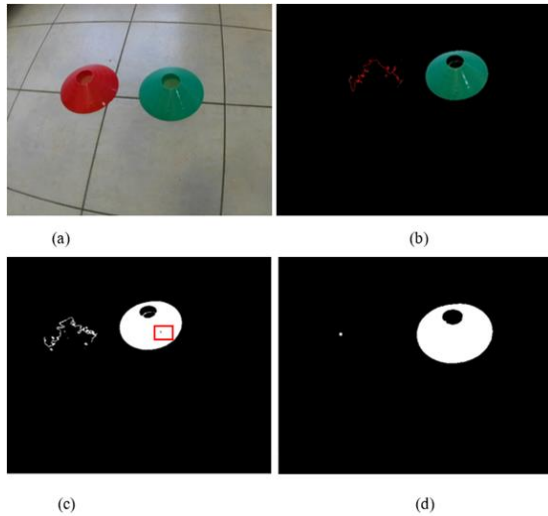


Figure 4 Original image (a), merged HSV threshold image and original image (b), threshold image in HSV without morphological (c) and with morphological operations (d) in an indoor environment.

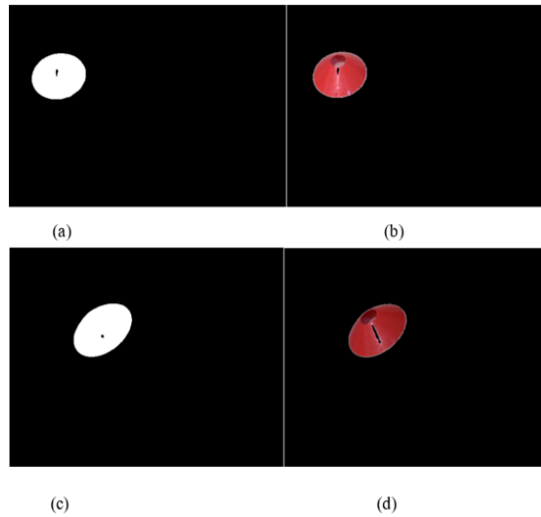


Figure 5 Threshold image in Lab with and without morphological operations (a) and (c) respectively. Merged threshold image in Lab and original image (b) and (d) in an indoor environment.

Table 1 Upper and lower threshold values in HSV and Lab

	Lower Values	Upper Values
Hue	85	95
Saturation	114	255
Value	77	255
Luminance	60	214
Chrominance A	152	255
Chrominance B	141	255

Figure 4d and Figure 5d illustrate the effectiveness of Gaussian filters in object detection. Green (green bounding box) and red (red bounding box) cones presented in the original image data in Figure 4a and Figure 5b, respectively, were detected with almost identical shape and size. It is known as a true positive of

two in this instance since two cones were presented and detected. Yellow dots indicate the centroid of the detected object. Whereas without a Gaussian filter, many objects were improperly detected, as evidenced by the presence of several extra bounding boxes in the same scenario as in Figure 6b. The presence of undesired noise led to false edge and colour detection. Consequently, false positives occurred when the objects were absent from the original data but appeared as detected. According to the experiment outcomes, Gaussian filters substantially smoothed image data and improved the edges detection as well as prevented false positives. In addition, the use of kernel size (5, 5) demonstrated high overall edge detection performance without compromising quality of image data.

Figure 4d and Figure 5d depict the significant improvement when applied morphological operations in obstacle detection compared to the ones without. There was an obvious enhancement in noise removal when applied this CV technique. It would enable CV to avoid inadvertent detection when objects were tiny and far away. Specifically, Figure 4c shows that a small portion of red cone was detected which could be an issue if applied to the same values of HSV during the deployment. The detection can simply be sunlight in the afternoon. Hence, the use of morphological operations improved obstacle detection, removed imperfections in the threshold images and delivered a fuller information on the structure of the image.

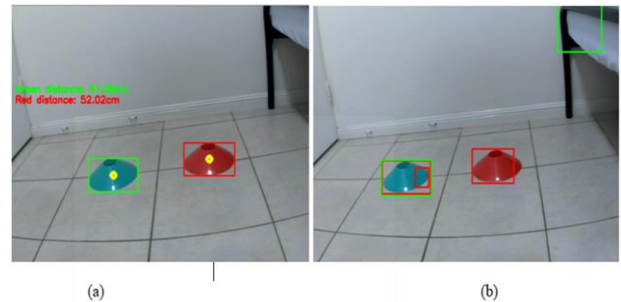


Figure 6 Object detection using Gaussian filter (a) and without Gaussian filter (b) (with all other mentioned CV techniques for both cases) in an indoor environment

## 2. Outdoor Object Detection Experiment Results

The proposed image based local path planning was deployed at Australian Institute of Marine Science in Townsville on James Cook University WAM-V as a trial before the 2022 Maritime RobotX competition. Figure 7 depicts WAM-V deployed on water with computer vision, GPS subsystem, and RPI's subsystems, Netgear N3000 router for communication between WAM-V and client PC.

The camera captured real time images of the robot’s workspace and tracks all the obstacles within its field of view. The camera sent all the image data to the Client PC. The path-planning algorithms then calculated the position data with the help of image data. After establishing wireless connection between robot and the client PC, the client program sent the heading position data to the WAM-V. The process was repeated until reaching the target.

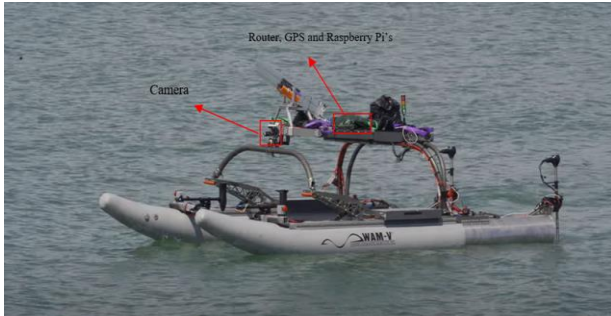


Figure 7 WAM-V on water during deployment.



Figure 8 Original image data without filtering.

The obstacle map consists of 1920 x 1080 cells during deployment and running at a constant rate of 50 Hz. However, the image size was reduced to 640x320 for efficiency purposes as. As the image was captured in the sea, the presence of waves and water reflection were challenging to detect the obstacles in that format. Especially, when the true colour of the buoys were affected due to sunlight and uneven illumination. This section will focus on object detection when using various CV techniques in Python with preliminary results in MATLAB. Specifically, it will compare the differences between when deployed the WAM-V in water with simulation in a video.

Figure 9 shows the effectiveness of HSV and Lab colour space selection when performing colour thresholding. Specifically, other objects were effectively eliminated

except green and red buoys via HSV and Lab colour thresholding technique, respectively. Threshold values for HSV and Lab are shown in Table 2. These values are subject to change with different environmental conditions.

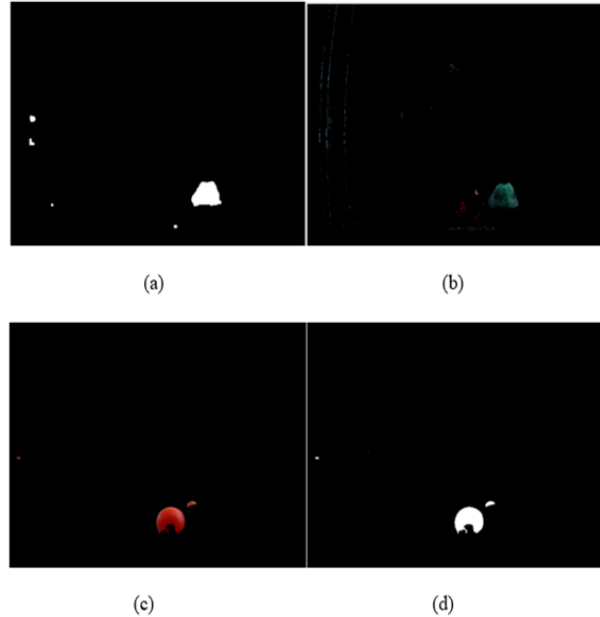


Figure 9 Threshold image using HSV (a), merged threshold HSV image and original image (b) and Lab colour space (c) merged threshold HSV image and original image (d).

Table 2 Outdoor upper and lower threshold values in HSV and Lab

	Lower Values	Upper Values
Hue	85	95
Saturation	114	255
Value	77	255
Luminance	60	214
Chrominance A	152	255
Chrominance B	141	255

Gaussian filter and colour-based segmentation would be useful to eliminate any background noise as well as other objects except red and green buoys. However, the captured image was firstly converted into HSV and Lab format before applying mentioned CV techniques. After colour-based segmentation, applied dilation function to remove noise. As shown in Figure 9, only green or red buoys were present. Subsequently, threshold images were combined in one frame and labelled with a bounding box around as shown in Figure 10. The green and red bounding box represented green and red buoy, respectively. The yellow dots indicated the centroid of detected objects.

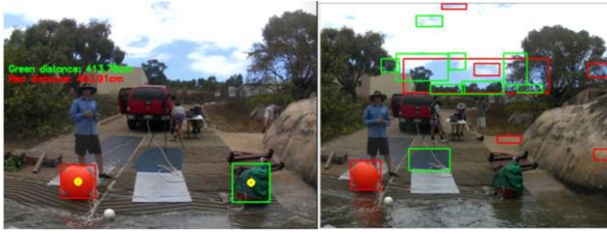


Figure 10 Object detection using Gaussian filter (a) and without Gaussian filter (b) (with all other mentioned CV techniques for both cases).

Figure 10a illustrates the effectiveness of the Gaussian filter in object detection. Red and green buoys were correctly detected with proper shape and features. In addition, the use of kernel size (5, 5) demonstrated high overall edge detection performance without compromising quality of image data. Both obstacles presented in the original image data were detected with almost identical shape and size. It is known as a true positive of two in this instance since two buoys were presented and detected. Whereas without a Gaussian filter, many objects were improperly detected, as evidenced by the presence of several extra bounding boxes in the same scenario as shown in Figure 4b. The presence of undesired noise led to false edge and colour detection. Consequently, false positives occurred when the objects were absent from the original data but appeared as detected. According to the experiment outcomes, Gaussian filter substantially smoothed image data and improved the edges detection as well as prevented false positives.

Even though not all characteristics of the buoys were detected, the WAM-V was still able to perform obstacle avoidance algorithm using APF since it was aware of obstacles in its path.

The preliminary obstacle detection in MATLAB faced many problems with water reflection that led to objects detected higher than expected. That could cause a greater issue if deployed on the WAM-V due to the obstacle detection subsystem would output a closer distance than expected. Consequently, the WAM-V might incorrectly perform obstacle avoidance earlier than expected and collide with the obstacles. The use of polarised lenses reduced water reflection and increased visual clarity of the buoys, particularly in bright conditions during deployment. From initial experimentation was almost no presence of water reflection in the image data. The buoys were detected with a similar shape and size. Consequently, the use of polarised lenses improved accuracy of distance estimation as well as path planning as a result.

### 3. Outdoor Path Planning Results

Higher level path planners can only be achieved if an accurate obstacle information is provided as well as its initial and target position. Since it was assumed that the initial and target position were provided, obstacle detection is critical for autonomous navigation in complex outdoor environments. Specifically, high accuracy of distance estimation was the most important factor that contributed to accurate position determination in path planning. This section will evaluate accuracy of distance estimation and behaviour of path planning trajectory with various distance variations.

The effectiveness of a single use camera is evaluated for distance estimation based on known height and distance from the camera in the reference image (see Table 3). For the experiments, an ELP-SUSB1080P01-L36 camera with IMX322 Sensor 0.01 Lux low illumination was used. To estimate distance, it was first to capture red buoy as a reference image (see Figure 11) to find the focal length of the camera using (1) because it was difficult to accurately measure the distance between camera and the buoy in water, hence, the focal length estimation was executed indoor instead. Subsequently, the distance could be estimated when deployed in water using (2). The result for distance estimation is shown in Figure 10a and Figure 12. The summary of distance estimation is shown in Table 3. It indicated that the measured and estimated distance were almost identical. There was only a small difference between these results which can be overcome by adding the difference small delta ( $\Delta x$ ) value to (2) as shown in (6). In this case the  $\Delta x$  was +13cm.

$$Estimated\ Distance = \frac{known\ height * focal\ length}{real\ time\ pixel\ height} + \Delta x \quad (6)$$



Figure 11 Reference image to estimate focal length and distance between red buoy and the camera.



Figure 12 Distance estimation using single camera.

Table 3 Green buoy specifications, measured and estimated distance.

Radius (cm)	Height (cm)	Measured Distance (cm)	Estimated Distance (cm)	Delta Value $\Delta x$ (cm)
50	60	400.78	413.78	+13
50	60	520	533	+13

4. Trajectory Evaluation

This section is to focus on obstacle avoidance and behaviour of the WAM-V trajectory. It was to consider the effectiveness of the APF algorithm if there were variations in distance between the two buoys. Specifically, each buoy was placed 6m apart so that the WAM-V would be expected to traverse in the middle of its trajectory. Whereas a side-by-side situation, it was expected the WAM-V to perform obstacle avoidance to divert itself away from the two obstacles. As shown in Figure 13a, the trajectory was successfully planned in between the two buoys which would expect the WAM-V to behave the same way because the distance between two buoys was twice its physical width. On the other hand, when the two buoys were side by side, the trajectory performed object avoidance on the left side of the two buoys towards the target position as shown in Figure 13b.

A new trajectory was updated with a sampling time of 100ms for running the algorithm in real time on the WAM-V; however, due to the existence of the asynchronous subsystem, a new trajectory is only recalculated every 2 seconds instead. However, the boat moved reasonably slow, it was expected the WAM-V to react responsively to obstacles within 3 seconds. Hence,

2 seconds update should allow enough time for the WAM-V to perform obstacle avoidance.

In both cases, the trajectories were not the shortest path from the initial position to the target, however, it planned the WAM-V to move along its path, modified its position and orientation as necessary to avoid collisions. Additionally, the path with two buoys side by side was not the smoothest possible solution during deployment. However, a local path planner using APF accomplished its goal by modifying the WAM-V configuration to minimise the potential on the robot and therefore attempted to eliminate collisions.

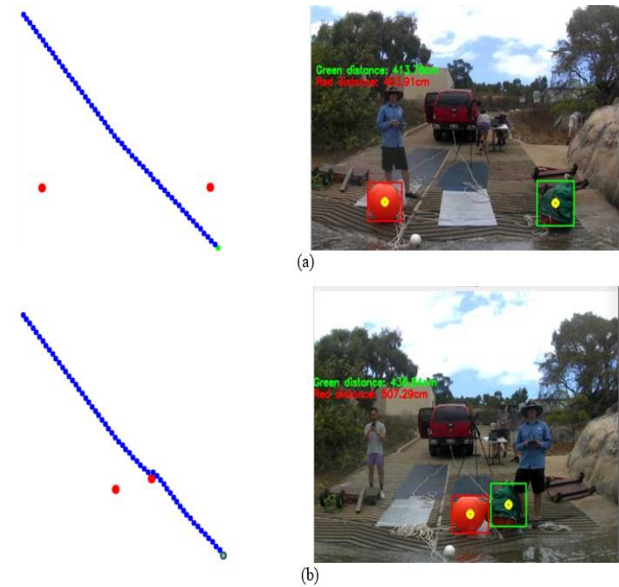


Figure 13 Detected objects (red dots) (a) and path planner when two buoys were 6m apart (b) and side by side (c) approaching the target position (green dot).

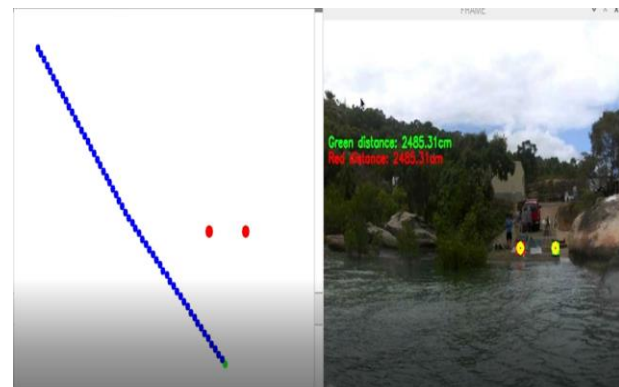


Figure 14 Detected buoys from far distance (24m).

Figure 14 indicates the effectiveness of the detection that could detect the buoys from approximately 24.8m and perform obstacle avoidance and adjusted trajectory at early stage. That would allow the WAM-V to have

enough time to adjust its heading, velocity and manoeuvre appropriately.

## V. PLATFORM ASSESSMENT AND FUTURE DEVELOPMENT

### A. McKeough USV

The integration of image processing and local path planning has been developed and tested on the WAM-V using various CV techniques to detect obstacles and APF for obstacle avoidance. In addition to reducing the need for expensive test facilities, the use of the model-free approach on stationary obstacles allowed for testing in open water, which was vital for real-world scenarios.

The project involved two main parts such as vision-based obstacle detection and local path planning. In the obstacle detection part, the WAM-V successfully detected most features and size of the green and red buoys. The use of polarised lenses vastly reduced the presence of water reflection, hence, the detected objects appeared without any increase in size due to water reflection. Consequently, the accuracy of distance estimation and path planning were also improved and optimised, respectively.

In path planning, the WAM-V also successfully performed obstacle avoidance when detected obstacles were 6m and side by side. When obstacles were 6m apart the trajectory traversed in between the detected buoys. Whereas when they were side by side, it performed obstacle avoidance and adjusted the trajectory. In both cases, the trajectory was not the shortest path possible, however, it enabled the WAM-V to reconfigure its original trajectory and attempted to eliminate collisions. However, at this stage there is no communication with the system identification subsystem, hence, it will be future work to communicate between two subsystems to autonomously guide the WAM-V.

Future work will focus on deployment of aforementioned image processing and local path planning on multiple obstacles. In addition, the successful obstacle avoidance on two buoys will provide opportunity to integrate with harmonic potential functions (HPFs) which is a special type of APF which solve the issue of local minima where the WAM-V is stuck in the same position over and over again. Furthermore, an 2D nonholonomic fluid motion planner will be applied with HPFs to plan a much smoother plan when performing obstacle avoidance.

### B. Parker UAV

The designed UAV presently has only been capable of manual hover flight. Due to delays in battery acquisition and other time and budget constraints, more advanced

control and testing of the design has not been able to be practically achieved. However, the design does provide a robust and simple platform for future integration within the multi domain scenario, with the ability to be reconfigured with different sensors.

Future improvement and development of the UAV will include progression of the autonomous control systems, HSI sensor integration, inclusion of the UAV Replenishment capability alongside on-vessel standby recharging. There is also potential for an alternate hybrid drone frame for longer distance flights.

## V. CONCLUSION

A variety of challenges arose in the lead up to competition. Many of these were indicative of the core challenges that define a task of this scale and range from standard system definition, identification and execution to logistical, administrative and organisational issues. Experiences such as these leave JCU Robotics better positioned to respond to challenges in future projects and competitions of the same broad-reaching scale.

## VI. ACKNOWLEDGEMENTS

JCU Robotics would like to thank Doctor Shou-Han Zhou for kick-starting and leading this project. Thanks for working so hard to try and wrangle our team of cats. The Parker-McKeough AMS is dedicated to the memory of our friends, Lochlan and Katrina.

## VI. REFERENCES

- [1] Y. K. Hwang, N. Ahuja, and others, "A potential field approach to path planning," *IEEE transactions on robotics and automation*, vol. 8, no. 1, pp. 23–32, 1992.
- [2] D. Lau, J. Eden, and D. Oetomo, "Fluid motion planner for nonholonomic 3-D mobile robots with kinematic constraints," *IEEE Transactions on Robotics*, vol. 31, no. 6, pp. 1537–1547, 2015.
- [3] NETGEAR Inc, *Wireless-N 300 Modem Router DGN2200 Setup Manual*. [Online]. Available: [https://www.downloads.netgear.com/files/GDC/DGN2200/DGN2200\\_SM\\_30Mar2010.pdf](https://www.downloads.netgear.com/files/GDC/DGN2200/DGN2200_SM_30Mar2010.pdf)